Jurnal Media Mesin, Vol. 27 No. 2
Printed ISSN: 1411-4348
Online ISSN: 2541-4577

PERFORMANCE EVALUATION OF A SMALL-SCALE LPG ALUMINIUM MELTING FURNACE USING FOUR-LAYER REFRACTORY INSULATION

Hariningsih
Program Studi D-IV Teknologi Rekayasa Perancangan Manufaktur
Politeknik Manufaktur Ceper, Klaten, Indonesia
Email: hariningsih@polmanceper.ac.id

Arif Syamsudin
Program Studi D-IV Teknologi Rekayasa Perancangan Manufaktur
Politeknik Manufaktur Ceper, Klaten, Indonesia
Email: arif@polmanceper.ac.id

Bangun Rifki Darmawan
Program Studi D-IV Teknologi Rekayasa Perancangan Manufaktur
Politeknik Manufaktur Ceper, Klaten, Indonesia
Email: bangunrifki123@gmail.com

ABSTRAK

Limbah aluminium yang berasal dari komponen otomotif dan mesin industri memiliki potensi besar untuk didaur ulang; namun, usaha kecil dan menengah (UKM) serta lembaga pendidikan vokasi masih memerlukan tanur peleburan yang ringkas dan efisien secara termal. Studi ini menjelaskan desain, analisis kinerja termal, dan pengujian eksperimental tanur peleburan aluminium berbahan bakar LPG dengan kapasitas 7 kg, yang dilengkapi dengan lapisan refraktori empat lapis yang terdiri dari ceramic fibre paper, ceramic fibre blanket, ceramic fibre board, dan LCF384A insulating castable. Tanur ini memiliki ruang bakar dengan diameter 280 mm dan tinggi 320 mm, serta krusibel baja berdiameter 165 mm dan tinggi 233 mm. Analisis termal menunjukkan bahwa krusibel memiliki volume efektif sebesar 3,49 dm³, yang setara dengan kapasitas 9,44 kg aluminium padat dan 8,05–8,24 kg aluminium cair. Lapisan refraktori berlapis banyak tersebut menghasilkan hambatan termal keseluruhan sebesar 0,809 K/W, yang menghasilkan estimasi kehilangan panas konduktif sekitar 1,195 kW pada suhu tanur 1000 °C. Enam uji coba peleburan dilakukan menggunakan limbah aluminium dari piston, blok mesin, dan mesin tekstil. Tanur tersebut berhasil melebur 7 kg aluminium dalam waktu 1380–1965 detik (23,0–32,8 menit) dengan konsumsi LPG antara 2,0–3,2 kg. Parameter pembakaran (λ) bervariasi antara 1,02–1,21, yang menunjukkan pembakaran yang stabil dan bersih. Spektroskopi emisi optik mengungkapkan bahwa paduan blok mesin dan piston hasil daur ulang memiliki komposisi kimia yang paling mendekati paduan aluminium cor komersial, meskipun penambahan Cu diperlukan untuk sepenuhnya memenuhi spesifikasi standar. Tanur yang diusulkan ini menunjukkan kinerja termal yang andal, kehilangan panas konduktif yang minimal, dan karakteristik peleburan yang stabil, sehingga ideal untuk pendidikan vokasi dan aplikasi pengecoran aluminium skala kecil.

Kata kunci: aluminium, daur ulang, peleburan, tungku, insulasi

ABSTRACT

Aluminium scrap derived from automotive and industrial machinery components holds considerable potential for recycling; however, small and medium enterprises (SMEs) and vocational institutions still need compact, thermally efficient melting furnaces. This study outlines the design, thermal performance analysis, and experimental assessment of a 7 kg LPG-fired aluminium melting furnace, which features a four-layer refractory lining made up of ceramic fibre *paper, ceramic fibre blanket, ceramic fibre board, and LCF384A insulating castable. The furnace includes a combustion chamber with a diameter of 280 mm and a height of 320 mm, along with a steel crucible that measures 165 mm in diameter and 233 mm in height. Thermal analysis indicated that the crucible offers an effective volume of 3.49 dm³, which corresponds to a capacity of 9.44 kg of solid aluminium and 8.05–8.24 kg of molten aluminium. The multilayer refractory lining achieved an overall thermal resistance of 0.809 K/W, leading to an estimated conductive heat loss of around 1.195 kW at a furnace temperature of 1000 °C. Six melting trials were performed using aluminium scrap from pistons, engine blocks, and textile machines. The furnace successfully melted 7 kg of aluminium within a time frame of 1380–1965 seconds (23.0–32.8 minutes) while consuming between 2.0 and 3.2 kg of LPG. The combustion parameter (λ) varied from 1.02 to 1.21, indicating stable and clean combustion. Optical emission spectroscopy revealed that the recycled engine block and piston alloys had chemical compositions that were closest to those of commercial casting aluminium alloys, although additional Cu is necessary to fully meet standard specifications. The proposed furnace exhibits dependable thermal performance, minimal conductive heat loss, and stable melting characteristics, making it ideal for vocational education and small-scale aluminium casting applications.*

Keywords: *aluminium, recycling, smelting, furnace, insulation*

1. INTRODUCTION

Aluminium serves as a non-ferrous metal that finds widespread use in the manufacturing, packaging, transportation, and machine component industries because of its exceptional heat conductivity, corrosion resistance, and lightweight nature. The growth in aluminium waste produced by household appliances, automobile parts, and beverage cans is closely correlated with the rise in aluminium usage. When compared to the manufacture from primary bauxite ore, the aluminium recycling process, which includes smelting (secondary aluminium), can save up to 95% of energy and drastically reduce CO_2 emissions [1]. Therefore, it is crucial to promote small and medium-sized businesses (SMEs) and vocational training by developing effective small-scale smelting technologies.

In the recycling process, conventional aluminium melting furnaces are essential because they heat aluminium scrap until it liquefies, enabling it to be recast or changed into new metal. Typically, this process begins with the gathering and sorting of scrap, which is followed by pretreatment stages including paint or oil coating removal, furnace charge, melting, alloying if necessary, and casting. Controlling the melting temperature and duration is essential for creating high-quality molten metal on a secondary industrial scale [2], [3], [4], [5].

Common forms of conventional furnaces include gas or oil-fired furnaces with a refractory lining to act as a heat barrier, rotary furnaces or rotating drums that improve the contact between the scrap and heat, and reverberatory furnaces, which reflect heat from the combustion chamber roof into the metal. The literature on modern aluminium furnace design has addressed these furnace concepts in great detail. The advantages of conventional furnaces include their capacity to treat a wide range of aluminium scrap, from cans and bales to automobile components, making them perfect for a variety of recycling applications. For large-scale applications, this technology has a wealth of operational data and is well-established. It also makes it easier to repeat batches of production consistently, which improves production stability. There are significant financial and environmental advantages to smelting aluminium for recycling [2][6][7].

However, there are a number of significant technical barriers and restrictions. Due to significant heat loss through the furnace walls or flue gases, thermal efficiency is typically low. Additionally, it can be difficult to maintain precise temperature control and process conditions, especially in small-scale operations, which can degrade the quality of the molten metal (for example, through oxidation, elevated dross levels, or inclusions). Stable temperature and smelting conditions are critical to the quality of aluminium scrap smelting and are sometimes difficult to maintain in smaller businesses. Furthermore, high emissions and waste residues from solid fuels or antiquated combustion processes cause environmental problems [2][8].

The design of aluminium melting furnaces has been the subject of numerous studies in the past. Mubarok et al. developed a 2 kg furnace that can melt aluminium in 15 minutes, but they omitted data on LPG gas use, which makes energy efficiency analysis more difficult [9]. Three distinct furnace capacities 5.739 kg, 3.77 kg, and 1.92 kg were tested by Shaleh and Tulloh. The largest capacity did not operate at its best, and only two of these reached the melting point in 25 to 30 minutes [10]. Aminur et al. built a 5 kg furnace that used 3 kg of LPG over 60 minutes, but they neglected to preheat the insulator, which affects energy consumption [11]. A similar furnace was designed by Mukhammad et al.; however their use of regular red brick as the main insulator resulted in a shorter service life and significant heat loss [12].

This study presented a novel design for an LPG-powered aluminium melting furnace with a 7 kg capacity. It uses LCF384A castable refractory cement, ceramic fibre paper, ceramic fibre blanket, and ceramic fibre board to create a four-layer thermal insulation system. The incorporation of refractory and insulating materials in furnace design is crucial for sustaining elevated internal temperatures while minimizing heat loss to the exterior wall. Comparable principles have been utilized in the engineering of high-temperature furnaces, where the choice and configuration of refractory materials play a significant role in influencing the thermal efficiency of the furnace [13]. To further enhance heat transfer to the crucible, the combustion system uses a combination of LPG and an air blower to produce an ideal stoichiometric mixture. The goal of this project is to create a furnace that can be used as a demonstration tool in vocational education labs and is suitable for the production requirements of small and medium-sized businesses (SMEs) by using a more integrated design approach. This invention could support downstream technology, improve student proficiency in casting techniques, and promote self-reliance in the country's metal sector.

2. METHOD

2.1 *Furnace Design*

Experimental studies were carried out utilizing a prototype aluminium melting furnace powered by LPG, which has a melting capacity of 7 kg. The furnace is composed of four primary components: the furnace body, a crucible, a refractory lining, and a combustion system, as depicted in Figure 1.

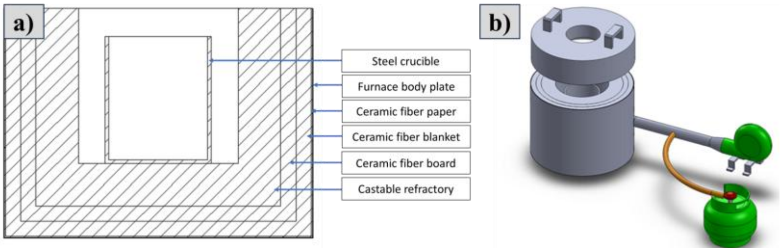

Figure 1. Furnace design: a) details of the insulation layer and b) furnace assembly

a. Furnace Body

The furnace body is made from a cylindrical steel drum measuring 520 mm in diameter, 350 mm in height, and featuring a wall thickness of 1 mm. The cover of the furnace includes a 180 mm filling hole that is positioned to align with the opening of the crucible. Once the refractory lining is installed, the dimensions of the combustion chamber are 280 mm in diameter and 320 mm in height.

b. Crucible

The crucible is fabricated from a steel pipe with an outer diameter of 168 mm, an inner diameter of 153 mm, an inner height of 226 mm, and an overall height of 233 mm. This crucible functions as a storage vessel for molten aluminium during the smelting operation.

c. Refractory Layers

The thermal insulation system features four refractory layers, positioned from the outer shell to the combustion chamber in the following order: 3 mm ceramic fibre paper, 65 mm LCF384A cast refractory, 25 mm ceramic fibre blanket, and 25 mm ceramic fibre board. This layered setup aims to decrease conductive heat loss and provide a consistent temperature throughout the furnace.

d. Combustion System

The furnace operates on LPG as its fuel, which is supplied via a high-pressure double-lock regulator (Winngas W191M). A 3-inch centrifugal blower provides the combustion air, achieving an airflow velocity of around 12 m/s when fully opened. The velocity of the airflow was assessed with a Benetech GM816 digital anemometer. The fuel and air are combined through the burner nozzle prior to entering the combustion chamber, facilitating stable combustion throughout the smelting process.

2.2 *Furnace Fabrication and Installation*

A prototype LPG-fired aluminum melting furnace with a capacity of 7 kg was constructed using a cylindrical design that comprises four primary components: the furnace body, refractory lining, cover, crucible, and burner system. The fabrication process consisted of several sequential stages, including material preparation, assembly of the furnace body, installation of the refractory, curing, and preheating. The insulation configuration of the furnace body and cover is illustrated in Figure 2, while the stages of preheating are depicted in Figure 3.

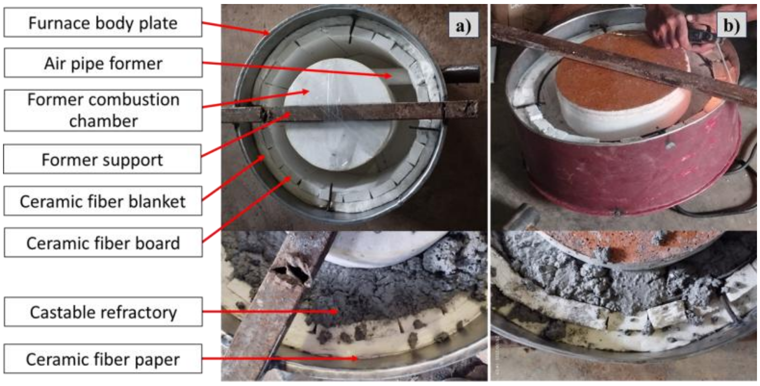

Figure 2. Insulation layer : a) body and b) cover

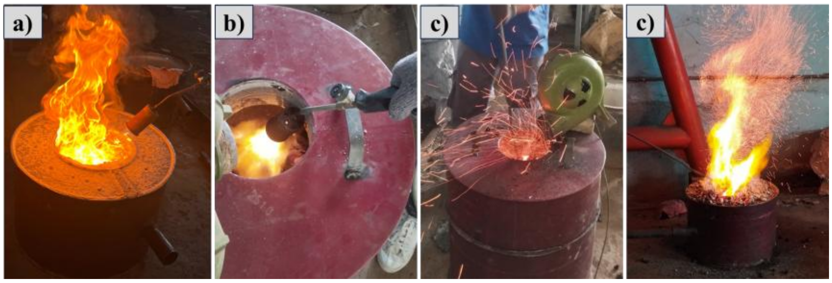

Figure 3. Preheating the furnace: a) burning former styrofoam, b) preliminary heating using a burner, c) additional heating with charcoal and a blower, and d) final heating

The materials utilized in the construction of the furnace included a steel drum for the outer shell, steel plates and pipes for structural elements, castable refractory (LCF384A), ceramic fiber paper, ceramic fiber blanket, ceramic fiber board, styrofoam, and concrete reinforcement. Initially, a styrofoam mold was created according to the specified geometry of the combustion chamber to shape the internal cavity, which included the burner passage and crucible location. The steel drum was then assembled and welded to create the furnace body, followed by the installation of the burner inlet and exhaust outlet.

The insulation system was established by applying layers of ceramic fibre to the inner surface of the steel shell prior to the casting of the refractory lining. A hand mixer was used to combine the castable refractory with water until a uniform consistency was achieved. This mixture was then poured into the furnace cavity and compacted around the styrofoam mold and concrete reinforcement. After a curing period of three days, the styrofoam mold was removed through a controlled firing process. The refractory lining was allowed to dry naturally for 21 days to reduce the risk of cracking due to moisture evaporation.

The furnace preheating was carried out using LPG combustion, supplemented by charcoal and forced air, for approximately six hours until the temperature reached around 900°C. This procedure was essential for eliminating residual moisture and enhancing the thermal stability of the refractory lining prior to conducting melting tests.

The crucible was constructed separately from a steel pipe, which was cut and welded to meet the specified dimensions. The final dimensions of the crucible were an outer diameter of 168 mm, an inner diameter of 153 mm, and an effective height of 190 mm (refer to Figure 4).

The steel crucible's capacity was assessed by computing its internal volume, utilizing the principles of cylindrical geometry. The volume of the crucible was determined using Equation (1):

$$\text{Volume (V)} = \pi r^2 t \quad (1)$$

where V represents the crucible volume (dm^3), r denotes the inner radius of the crucible (dm), and h indicates the inner height of the crucible (dm).

Subsequently, the maximum capacity for aluminium was estimated by applying the relationship between volume and material density, as expressed in Equation (2):

$$\text{Capacity (m)} = \rho \text{ V} \quad (2)$$

where m signifies the mass of aluminium (kg), ρ represents the density of molten aluminium (approximately 2.7 kg/dm^3), and V is the volume of the crucible (dm^3).

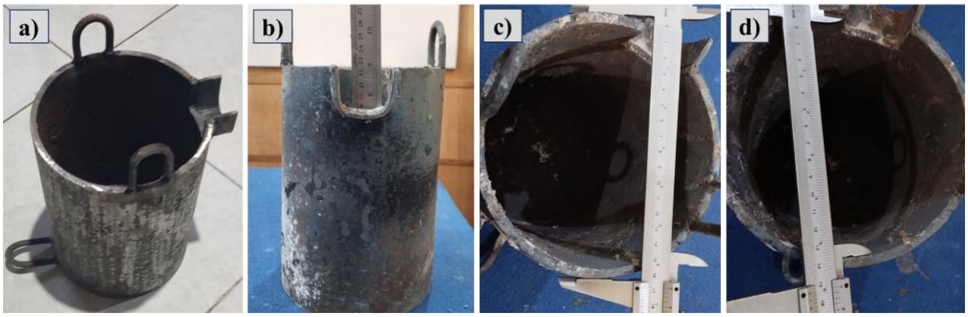

Figure 4. Steel crucible: a) full view, b) effective height 190 mm, c) outer diameter 168 mm, and d) inner diameter 153 mm

2.3 The Furnace Performance Test

The performance of the constructed LPG crucible furnace was assessed through six aluminium melting trials, each utilizing a consistent charge of 7 kg. The aluminium feedstock comprised industrial scrap sourced from various origins (Figure 5), specifically (a) used pistons, (b) engine blocks, (c) loom machine components, (d) a combination of engine blocks and pistons, (e) a blend of loom machine parts and pistons, and (f) a mixture of engine blocks and loom machine components. These material selections were made to reflect the typical aluminium waste found in small- and medium-sized foundry operations.

Figure 5. Aluminium waste: a) pistons, b) piston and engine blocks, c) piston and loom, d) engine blocks, e) engine block and loom, and 6) loom

Throughout each trial, the furnace was operated under uniform conditions to maintain experimental integrity. The blower valve was fully opened, generating an airflow velocity of around 12 m/s, while the LPG regulator valve was set to an opening angle of 135°. The temperature of the furnace was continuously monitored during the melting process using an Intel Safe JT-1450C infrared thermometer until the aluminum charge was completely melted.

Once melting was completed, the molten aluminum was poured into a greensand mold. The mold was created by combining silica sand with 10 wt.% bentonite as a binder and 4 wt.% water as a moisture activator [14], [15], [16]. The greensand molding technique was chosen as it reflects the traditional casting methods commonly used in small-scale foundries and vocational manufacturing workshops.

The evaluation of furnace performance was based on several critical indicators, including melting duration, LPG fuel usage, thermal stability, combustion efficiency, and the air-fuel ratio. These metrics were utilized to analyze the operational performance and energy efficiency of the developed furnace under varying conditions of aluminium scrap. The composition of the smelted aluminium was verified with a Bruker OES Q2 spectrometer. The chemical makeup of recycled aluminium can differ significantly based on its initial use and the source of the alloy. Consequently, analyzing the chemical composition is essential to determine the possible alloy grade and assess the appropriateness of recycled aluminium for future casting applications.

2.4 *Combustion Analysis*

The combustion characteristics were assessed by calculating the crucible's volume and capacity, airflow rate, fuel-to-air ratio (FAR), air-to-fuel ratio (AFR), and excess air coefficient (λ). The volume and capacity of the crucible were determined using Equations (1) and (2), respectively, while the pipe's cross-sectional area was computed with Equation (3). The total air mass flow rate during the melting process was subsequently derived using Equation (4). Utilizing the measured fuel consumption alongside the calculated airflow rate, the fuel-to-air ratio (FAR) and air-to-fuel ratio (AFR) were established through Equation (5), while the excess air coefficient (λ) was calculated with Equation (6) to assess the combustion conditions within the furnace.

The blower outlet cross-sectional area was calculated as

$$A = \frac{\pi d^2}{4} \tag{3}$$

where A is the outlet area (mm²) and d is the outlet diameter (mm).

The air mass flow rate and total air mass during melting were calculated by

$$m_{\text{air}} = \dot{m} \times t = \rho \, A \, v \, t \tag{4}$$

where ρ is the air density (kg/m³), V is the air velocity (m/s), and t is the melting time (s).

The fuel-to-air ratio (FAR) and air-to-fuel ratio (AFR) were determined by

$$\text{FAR} = \frac{m_{\text{fuel}}}{m_{\text{air}}}, \text{AFR} = \frac{m_{\text{air}}}{m_{\text{fuel}}} \tag{5}$$

Finally, the excess air coefficient was calculated as

$$\lambda = \frac{\text{AFR}_{\text{aktual}}}{\text{AFR}_{\text{stoik}}} \tag{6}$$

where $\text{AFR}_{\text{actual}}$ is the measured air-to-fuel ratio and $\text{AFR}_{\text{stoichiometric}}$ is the theoretical stoichiometric air-to-fuel ratio for LPG combustion.

2.5 *Thermal Resistance Analysis*

An analysis of thermal resistance was conducted to assess the insulation efficiency of the LPG crucible furnace. It was assumed that heat transfer through the furnace wall takes place via one-dimensional steady-state radial conduction across concentric layers of insulation, which include insulating castable, ceramic fibre board, ceramic fibre blanket, ceramic fibre paper, and an outer steel shell. The conductive thermal resistance for each layer was determined using Fourier's law applicable to a hollow cylinder as follows [17][18] :

$$R_{\text{wall},i} = \frac{\ln (r_o/r_i)}{2\pi k_i L} \tag{7}$$

In this context, ri and ro represent the inner and outer radii of the layer, respectively, while ki denotes the thermal conductivity and L signifies the height of the furnace. The total conductive resistance was calculated by adding the resistances of all insulation layers that are arranged in series. Following this, the convective and radiative thermal resistances at the outer surface of the furnace were incorporated to ascertain the overall thermal resistance, which was then utilized to estimate the heat loss from the furnace. The thermal conductivity of each lining material significantly influences the overall resistance to heat transfer. Materials that exhibit lower thermal conductivity offer enhanced resistance to conductive heat transfer, which in turn aids in reducing heat loss from the furnace chamber [19]. Table 1 below displays the thermal properties of materials used for furnace linings.

Table 1. Thermal properties of furnace lining materials

Layer	Thickness (mm)	Thermal conductivity (W/mK)
Steel shell	1	45 [20]
Ceramic fibre paper	3	0.12 [21]
Castable LCF384A	65	1.87 [22][23]
Ceramic fibre blanket	25	0.16 [24]
Ceramic fibre board	25	0.18 [25]

3. RESULTS AND DISCUSSION

3.1 *Thermal Resistance Analysis*

The thermal resistance of the multilayer furnace lining was assessed to determine its effectiveness in retaining heat within the combustion chamber. This evaluation included the side wall, bottom, and top cover, with the thermal resistance of each layer calculated based on its thickness and thermal conductivity. Additionally, the impact of each layer on the thermal resistance of the corresponding furnace section was analyzed. The findings are detailed in Tables 2–4, and the overall thermal resistance is compiled in Table 5.

The analysis of thermal resistance yielded a total thermal resistance of 0.809 K/W, derived from the parallel heat-transfer pathways through the furnace's side wall, bottom, and top cover. The bottom and top cover demonstrated greater thermal resistances of 7.264 and 12.158 K/W, respectively, while the side wall had a lower resistance of 0.983 K/W, attributed to its larger heat-transfer area. The ceramic fiber board and blanket significantly enhanced the insulation performance due to their comparatively low thermal conductivities of 0.15 and 0.12 W/m·K, respectively.

The measured thermal resistance demonstrates that the multilayer lining effectively resists conductive heat transfer from the 1000°C combustion chamber to the environment. With a temperature difference of 966 K, the estimated conductive heat loss was around 1.195 kW. Minimizing conductive heat loss aids in preserving thermal energy within the furnace, enabling a larger portion of the supplied heat to be utilized for the aluminium charge. This aligns with earlier research indicating that suitable refractory and insulation designs can decrease heat loss in furnaces and enhance the thermal efficiency of aluminium melting processes [26][27]. Additionally, better heat retention can lead to reduced melting times and decreased fuel usage, although the melting efficiency is also influenced by burner performance, heat transfer dynamics, and the operational conditions of the furnace [28].

Table 2. Thermal resistance of each insulation layer side wall

Layer	R (K/W)	Contribution (%)
Castable	0.101	10.3
Ceramic fibre board	0.382	38.8
Ceramic fibre blanket	0.428	43.5
Ceramic fibre paper	0.073	7.4
Carbon steel	0.00004	0.0
Total side wall	0.983	100

Table 3. Thermal resistance of each insulation layer bottom

Layer	R (K/W)	Contribution (%)
Castable	0.565	7.8
Ceramic fibre board	2.707	37.3
Ceramic fibre blanket	3.383	46.6
Ceramic fibre paper	0.609	8.4
Carbon steel	0.00036	0.0
Total bottom	7.264	100

Table 4. Thermal resistance of each insulation layer top cover

Layer	R (K/W)	Contribution (%)
Castable	0.740	6.1
Ceramic fibre board	4.613	37.9
Ceramic fibre blanket	5.767	47.4
Ceramic fibre paper	1.038	8.5
Carbon steel	0.00062	0.0
Total top cover	12.158	100

Table 5. Summary of thermal resistance analysis

Parameter	Value
Combustion chamber diameter	280 mm
Combustion chamber height	320 mm
Filling hole diameter	180 mm
Furnace temperature	1000 °C
Ambient temperature	34 °C
Temperature difference, ΔT	966 K
Side-wall thermal resistance, R_{wall}	0.983 K/W
Bottom thermal resistance, R_{bottom}	7.264 K/W
Top-cover thermal resistance, R_{top}	12.158 K/W
Overall thermal resistance, R_{total}	0.809 K/W
Estimated conductive heat loss, Q	1.195

3.2 *Steel Crucible Capacity and Performance*

The steel crucible, as depicted in Figure 4, was fabricated with an effective height of 190 mm, an outer diameter of 168 mm, and an inner diameter of 153 mm. Utilizing these measurements, the effective internal volume was determined through the cylindrical volume formula. The capacity of the crucible was then estimated by applying the densities of solid aluminium and molten aluminium at the melting temperature of 660.32°C. The results of these calculations are presented in Table 6.

Table 6. Calculated Dimensions and Capacity of the Steel Crucible

Parameter	Value
Effective height	190 mm
Inner diameter	153 mm
Outer diameter	168 mm
Effective volume	3.49 dm^3
Solid aluminium density	2.70 g/cm^3
Molten aluminium density (Ref. [29])	2.357 g/cm^3
Molten aluminium density (Ref. [30])	2.304 g/cm^3
Calculated capacity (solid aluminium)	9.435 kg
Calculated capacity (molten aluminium, Ref. [29])	8.237 kg
Calculated capacity (molten aluminium, Ref. [30])	8.05 kg

The analysis reveals that the crucible has an effective volume of about 3.49 dm^3, which translates to a capacity of roughly 9.435 kg for solid aluminium and between 8.05 and 8.237 kg for molten aluminium, depending on the reference liquid density used [29][30]. While there are minor discrepancies in the reported liquid densities, the resulting variation in capacity is minimal, affirming that the designed crucible meets the intended nominal melting capacity of around 7 kg. This capacity is deemed sufficient for laboratory-scale experiments and small-scale aluminium recycling activities.

Throughout the operation of the furnace, the steel crucible demonstrated commendable structural integrity, showing no significant deformation or cracking even after multiple heating cycles. The exceptional mechanical strength and thermal shock resistance of steel render it ideal for open-flame melting furnaces that utilize LPG fuel. Moreover, steel crucibles can be produced locally through standard welding techniques, which makes them considerably more cost-effective compared to commercial graphite crucibles. These features are especially beneficial for small and medium enterprises (SMEs), vocational labs, and educational institutions, where the affordability of equipment and ease of fabrication are critical factors.

In comparison to graphite crucibles, steel exhibits superior resistance to mechanical impacts and repeated thermal cycling. While a thin Fe–Al intermetallic layer can form at the junction of molten aluminium and the steel surface, this layer develops slowly and usually results in minimal contamination during short- to medium-term use. On the other hand, graphite crucibles are more prone to oxidation at high temperatures and generally incur higher manufacturing costs along with more specialized production methods [31][32]. Consequently, for the furnace designed in this study, a steel crucible represents a practical balance between fabrication expenses, durability, and melting efficiency.

3.3 *Melting Time and Fuel Consumption*

The furnace operating parameters are shown in Figure 6. The furnace operates by fully opening the blower valve, allowing the air flow velocity into the furnace to reach 12 m/s (Figure 6.b). The fuel supply utilizes a high-pressure LPG regulator with a valve opening of 135° (Figure 6.c), while the LPG cylinder is partially submerged in water to mitigate extreme temperature drops caused by the Joule-Thomson effect, which can lead to gas freezing and flow restriction. Under these circumstances, the most stable flame is blue-green (Figure 7.a), signifying a nearly ideal air-fuel ratio (see the results of the AFR calculation in Table 7). If the air flow is decreased or the LPG regulator opening is lessened, the flame will turn red due to an unbalanced combustion ratio.

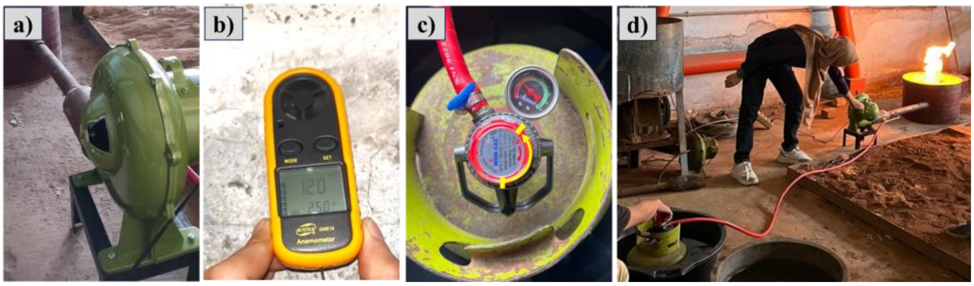

Figure 6. Operating parameters of the furnace: a) blower fan completely opened, b) air velocity at 12 m/s, c) LPG gas valve opened to 135°, and d) LPG gas submerged in water

The blue-green flame observed during combustion (Figure 7.a), typical of an LPG system with an optimal fuel-air mixture, indicates nearly perfect combustion, resulting in minimal soot production and low CO/hydrocarbon emissions. The primary benefits of this condition include enhanced thermal efficiency, reduced emissions, and improved temperature stability and control within the combustion chamber. Consequently, the presence of a blue flame can act as a visual cue that the combustion system (including the burner, airflow, and fuel ratio) is functioning correctly. For instance, Amrenova (2025) discovered that at equivalence ratios near unity, a blue flame consistently emerges, producing the lowest CO concentrations [33]. Likewise, studies on high-temperature water combustion reveal that a blue/greenish flame appears under very clean combustion conditions and high temperatures, which correlates with more efficient heat distribution [34].

LPG gas can lead to freezing in high-pressure regulators due to gas expansion and the heat-absorbing nature of vaporization: as LPG (propane/butane) transitions from high to low pressure within the regulator, it experiences rapid cooling that can lower the surface temperature of the regulator significantly below freezing, particularly during high flow rates or when steam/moisture is present in the gas. Furthermore, water vapor or other impurities can crystallize or create hydrates that obstruct the lines, which speeds up the freezing process. To mitigate this, immersing the regulator section or the post-regulation line in a water bath heater offers an external heat source and thermal mass that provides the enthalpy of vaporization for the LPG, thereby preventing the temperature from falling below freezing, ensuring stable pressure and vaporization rates, and minimizing the likelihood of ice formation or hydration within the regulator [35][36].

Throughout the melting process, as aluminium attains an ideal liquid state, the furnace's peak temperature is noted to be 1003°C (Figure 7.b). When tapping occurs, the molten aluminium's temperature is approximately 784.2°C, while during the pouring phase, it measures 737°C. Figure 7.c illustrates that with a load of 7 kg of aluminium scrap, the molten aluminium in the crucible has not yet reached its effective height or is not completely full. This suggests that the crucible still has the capacity to hold more than 7 kg. Originally, this crucible was intended for a capacity of 7 kg, but its dimensions were subsequently increased slightly to allow for a maximum load of 8 kg (refer to the calculation of the crucible capacity in Tabel 6.) to ensure adequate space and mitigate the risk of molten aluminium overflow.

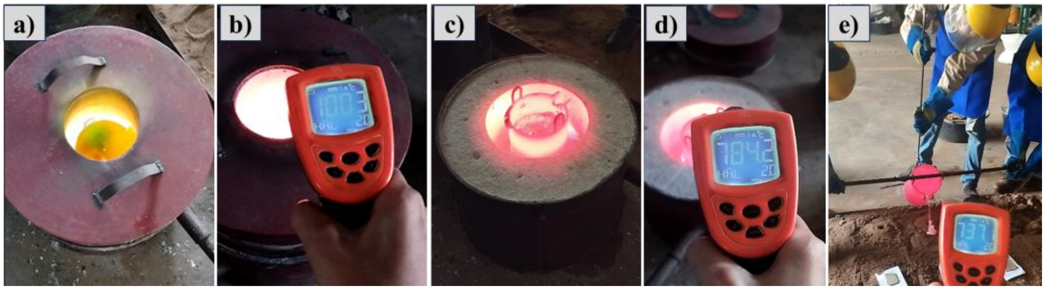

Figure 7. Melting test: a) green flame, b) peak temperature of 1003°C, c) available crucible capacity, d) tapping temperature 784.2 °C, and e) pouring temperature 737 °C

The air mass, fuel-air ratio (FAR), air-fuel ratio (AFR), and lambda value (λ) for each melting experiment were calculated using Eqs. (1)–(5). The calculated results are summarized in Table 7.

Table 7. Air fuel ratio based on experimental results

Material	Processing time (s)		Fuel (kg)	Air mass during operation (kg)	Air fuel ratio (AFR)		Fuel air ratio (FAR)	Lambda (λ)	Melting rate kg/jam
	Completely melted	Ready to pour			Fuel	Air			
P	1800	1965	3.219	51.224	1	15.913	0.0628	1.02	12.82
PE	1620	1852	2.564	48.278	1	18.829	0.0531	1.21	13.61
L	1645	1728	2.717	45.046	1	16.579	0.0603	1.06	14.58
E	1560	1722	2.444	44.889	1	18.367	0.0544	1.18	14.63
EL	1200	1380	2.051	35.974	1	17.540	0.0570	1.12	18.26
PL	1660	1757	2.610	45.802	1	17.549	0.0570	1.12	14.34
Average	1581	1734	2.601	45.202	1	17.463	0.0575	1.12	14,71

Note: P = piston; E = engine block; L = loom machine components; PE = piston and engine block; PL = piston and loom machine components; EL = engine block and loom machine components

The results of the calculation of air mass, fuel-air ratio (FAR), air-fuel ratio (AFR), and lambda value (λ) are presented in Table 1. The stoichiometric air-fuel ratio (AFR) for LPG (propane/butane) falls within the range of 15.6–15.8:1 [37]. According to the calculations presented in Table 1, the experimental AFR varies from 15.913–18.829:1, while the lambda (λ) value spans from 1.02 to 1.21.

The λ (lambda) value represents the ratio of the actual air-fuel ratio to the stoichiometric air-fuel ratio for a specific fuel. A λ value of 1 signifies a stoichiometric mixture, $\lambda < 1$ indicates a fuel-rich mixture (deficient in air), and $\lambda > 1$ denotes a fuel-lean mixture (excess air) [38]. In industrial furnaces operating under high pressure and temperature conditions, it is standard practice to maintain an excess air level of about 10–20% (i.e., $\lambda \approx 1.10$–1.20) during high fire to mitigate CO and soot production while ensuring thermal efficiency. In tightly controlled process applications, the ideal excess air may be lower (approximately 8–10%, $\lambda \approx 1.08$–1.10). This range serves as a general guideline frequently utilized in the tuning of industrial burners.

If the λ value is less than 1, the mixture is considered relatively rich, which poses a risk of elevated CO levels, soot production, unstable flames, and reduced heat transfer efficiency. This condition is particularly harmful to the quality of the molten metal surface during metal melting [33][39]. Conversely, when the λ value is slightly greater than 1, the mixture becomes slightly lean, resulting in cleaner combustion (characterized by a blue flame) and lower CO emissions. Notably, all melting test results indicate a λ value exceeding 1, specifically ranging from 1.02 to 1.21. This suggests that combustion is both stable and clean. According to the U.S. Department of Energy, a λ value of approximately 1.05 to 1.15 is often regarded as an optimal balance for small melting furnaces, ensuring flame cleanliness, high temperatures, and efficiency. However, if the excess air is excessively high (with λ significantly greater than 1.10 to 1.20), heat is wasted on heating the surplus air, leading to decreased efficiency and an increased risk of NO_x formation at elevated temperatures [40][41].

3.4 *Chemical composition of recycled aluminium*

Table 8 illustrates the chemical compositions of recycled aluminium from different scrap sources and their corresponding alloy references. The results highlight significant variations in the amounts of Si, Cu, Mg, Zn, and other alloying elements. Scrap E and P had relatively high Si levels of 10.61 and 10.11 wt.%, respectively, indicating a resemblance to Al-Si casting alloys like AC8C, A380, and AC4B. Scrap L recorded the highest Zn content at 4.465 wt.%, closely aligning with the 7075 alloy. In contrast, PL and EL were nearest to AC4D, while PE showed a composition that was closest to AC4B. These differences suggest that the scrap came from different alloy systems and may have varying melting behaviors.

Table 8. Chemical composition of recycled aluminium from various scrap sources

Scrap	Chemical composition (%)										Closest alloy reference
	Si	Fe	Cu	Mn	Mg	Cr	Ni	Zn	Ti	Al	
E	10.61	0.546	1.776	0.297	0.105	0.024	0.045	0.242	0.053	86.19	AC8C/A380
P	10.11	0.519	1.774	0.157	0.751	0.028	0.393	0.945	0.039	85.17	AC4B/AC8C
L	2.869	0.403	2.546	0.082	0.223	0.011	0.033	4.465	0.101	89.05	7075
PL	6.715	0.348	1.766	0.173	0.432	0.011	0.175	4.005	0.064	86.18	AC4D
EL	5.847	0.392	1.902	0.205	0.209	0.014	0.021	2.148	0.068	89.06	AC4D
PE	9.364	0.524	2.819	0.253	0.237	0.022	0.134	0.765	0.089	85.58	AC4B

The piston scrap (P) had a silicon content of 10.11 wt.% and was most similar to AC4B/AC8C. Despite this significant Si percentage, it experienced the longest melting duration. This suggests that the melting time was influenced by factors beyond just the chemical composition. The piston's relatively large and compact design, with a diameter of around 150 mm, resulted in a lower surface-area-to-volume ratio, which restricted heat transfer to the core and extended the melting time.

In contrast, the engine block scrap (E) demonstrated the shortest melting duration. Its silicon content was slightly higher at 10.61 wt.%, aligning with Al-Si casting alloys, while its fragmented shape offered a greater exposed surface area. This increased heat transfer from the furnace to the scrap, leading to quicker melting. Consequently, the melting behavior was shaped by the interplay of chemical composition, scrap geometry, and heat transfer, rather than being dictated by chemical composition alone.

4. CONCLUSION

This research successfully designed and assessed a 7 kg-capacity LPG-fired aluminum melting furnace, which features a four-layer refractory insulation system made up of ceramic fiber paper, ceramic fiber blanket, ceramic fiber board, and insulating castable. Thermal analysis indicated that the steel crucible has an effective volume of 3.49 dm³, equating to a capacity of 9.44 kg of solid aluminum and roughly 8.05–8.24 kg of molten aluminum. The refractory system delivered an overall thermal resistance of 0.809 K/W, leading to an estimated conductive heat loss of about 1.195 kW at a furnace temperature of 1000 °C.

Results from six melting trials indicated that the furnace reliably melted 7 kg of recycled aluminium in a time frame of 1380–1965 seconds (23.0–32.8 minutes), with LPG consumption ranging from 2.0 to 3.2 kg. The excess-air ratio (λ) varied between 1.02 and 1.21, suggesting stable combustion conditions. Analysis of the chemical composition through optical emission spectroscopy revealed that the recycled aluminium alloys from pistons and engine blocks were the most similar to commercial casting aluminium alloys among the scrap sources examined, although additional copper would be necessary to fulfill the relevant alloy specifications.

The furnace developed exhibited dependable thermal performance, minimal conductive heat loss, stable combustion, and uniform aluminium melting properties. By integrating thermal resistance analysis with experimental melting trials, a practical method for assessing the performance of small-scale LPG furnaces has been established. Consequently, this furnace is well-suited for small-scale aluminium casting and vocational education purposes, especially for illustrating combustion, heat transfer, refractory insulation, and aluminium recycling processes. Future research should concentrate on automatic temperature regulation, the long-term durability of refractories, numerical analysis of the thermal field within the furnace, and melt treatment to enhance both furnace efficiency and aluminium quality.

ACKNOWLEDGEMENT

The author wishes to extend their appreciation to the Directorate General of Research and Development of the Ministry of Higher Education, Science, and Technology of the Republic of Indonesia for providing funding for this research.

REFERENCES

[1] Berger R. New IAI study reveals environmental benefits of increased global aluminium can recycling [Internet]. International Aluminium Institute; 2025 [cited 2025 Jun 22]. Available from: https://international-aluminium.org/new-iai-study-reveals-environmental-benefits-of-increased-global-aluminium-can-recycling/
[2] Capuzzi S, Timelli G. Preparation and melting of scrap in aluminum recycling: a review. Metals (Basel). 2018;8(4):249. doi:10.3390/met8040249.
[3] Palacz M, et al. Experimental analysis of the aluminium melting process in industrial cold crucible furnaces. Met Mater Int. 2020;26(5):695-707. doi:10.1007/s12540-019-00368-2.
[4] Ieremenko I. Comparison of energy efficiency between existing and modern. 2022.
[5] Belt C. Current state of aluminum melting and holding furnaces in industry. JOM. 2015;67(11):2690-2695. doi:10.1007/s11837-015-1599-x.
[6] Brough D, Jouhara H. The aluminium industry: a review on state-of-the-art technologies, environmental impacts and possibilities for waste heat recovery. Int J Thermofluids. 2020;1-2:100007. doi:10.1016/j.ijft.2019.100007.
[7] Al-Alimi S, et al. Recycling aluminium for sustainable development: a review of different processing technologies in green manufacturing. Results Eng. 2024;23:25-66. doi:10.1016/j.rineng.2024.102566.

[8] Padamata SK, Yasinskiy A, Polyakov P. A review of secondary aluminum production and its byproducts. JOM. 2021;73(9):2603-2614. doi:10.1007/s11837-021-04802-y.
[9] Mubarok AA, Ilham MM, Fauzi AS. Rancang bangun metal foundry limbah aluminium bekas berkapasitas 2 kg berbahan bakar gas LPG. In: Seminar Nasional Inovasi Teknologi; 2020. p.317-322. Available from: http://repository.unpkediri.ac.id/2295/
[10] Shaleh M, Tulloh MH. Volume ruang bakar pada rancang bangun tungku peleburan aluminium skala laboratorium bahan bakar LPG. Ekliptika. 2020;1(1):37-49. doi:10.55757/ekliptika.v1i1.207.
[11] Aminur A, et al. Rancang bangun dan uji coba tungku krusibel dari tabung gas bekas dengan menggunakan sumber panas gas LPG. J Teknol Ter. 2020;6(2):118. doi:10.31884/jtt.v6i2.258.
[12] Mukhammad AFH, Ariwibowo D, Syarifucin YT, Robbaanii MA, Arifin Z, Yuliyanti Y. Pengujian awal kinerja tungku pengecoran logam aluminium matrix composite dengan bahan bakar gas LPG. Rotasi. 2016;18(4):110-116. doi:10.14710/rotasi.18.4.110-116.
[13] Purwanto D, Nasa RA. Perancangan tungku pemanas dengan menggunakan Kanthal A1. Media Mesin Maj Tek Mesin. 2021;22(1):13-21. doi:10.23917/mesin.v22i1.12462.
[14] Hariningsih, Lia N, Umardani Y. Optimalisasi komposisi pasir cetak green sand sebagai upaya menghilangkan cacat blow holes. J Foundry. 2022;5(2):23-29.
[15] Hariningsih H, Rizka T. Pengaruh penggunaan debu terhadap sifat mekanik pasir cetak greensand dengan bahan dasar pasir silika baru. Perwira J Sci Eng. 2015;5(1):1-4.
[16] Hariningsih H, Priandana DA, Awaludin M. Pengaruh penggunaan starch tapioka sebagai aditif pada pasir cetak greensand. J Foundry. 2023;6(1):16-23.
[17] Fu L, et al. Design, fabrication and properties of lightweight wear lining refractories: a review. J Eur Ceram Soc. 2022;42(3):744-763. doi:10.1016/j.jeurceramsoc.2021.11.019.
[18] Incropera FP, DeWitt DP, Bergman TL, Lavine AS. Fundamentals of heat and mass transfer. 6th ed. United States of America: John Wiley & Sons; 2007.
[19] Sari HN, Nurjannah I, Arsana IM, Dana GA, Julianto MV. The effect of temperature variation and various metal materials on conduction heat transfer rate. Media Mesin Maj Tek Mesin. 2023;24(2):102-108. doi:10.23917/mesin.v24i2.21138.
[20] Lamet, et al. Casting. In: ASM handbook. Vol. 15. Ohio: ASM International; 1988.
[21] Kerui Refractory. Ceramic fiber products [Internet]. 2026 [cited 2026 Aug 4]. Available from: https://keruiref.com/ceramic-fiber-paper/
[22] A.M. Products. Product bulletin LCF 384A. Ohio: A.M. Products; 2005.
[23] Bangkok Seng Thai Ltd., Part. Castable [Internet]. Bangkok: Bangkok Seng Thai Ltd., Part; [cited 2026 Aug 7]. Available from: https://www.bst-refractories.com/castable/
[24] C. Material. Ceramic fiber blanket. Pennsylvania; 2026. V. Refractories. Ceramic fiber board. Kalyan West; 2009.
[26] Saldívar AAF, Martínez RJ, Valdés AF, Torres JT, Palacios RMO, Li Y. Mathematical modelling for furnace design refining molten aluminum. Metals (Basel). 2021;11:1798. doi:10.3390/met11111798.
[27] Carmona M, Cortés C. Numerical simulation of a secondary aluminum melting furnace heated by a plasma torch. J Mater Process Technol. 2014;214(2):334-346. doi:10.1016/j.jmatprotec.2013.09.024.
[28] Qiu L, Feng Y, Chen Z, Li Y, Zhang X. Numerical simulation and optimization of the melting process for the regenerative aluminum melting furnace. Appl Therm Eng. 2018. doi:10.1016/j.applthermaleng.2018.09.060.
[29] Gray T. Liquid density of the elements [Internet]. Wolfram Research, Inc.; [cited 2025 Sep 29]. Available from: https://periodictable.com/Properties/A/LiquidDensity.al.html
[30] Spira N. Importance of aluminium density [Internet]. Kloeckner Metals Corporation; [cited 2025 Sep 29]. Available from: https://www.kloecknermetals.com/blog/why-is-the-density-of-aluminum-important/

[31] Kwon H. Chemical reaction between aluminium and graphite crucible during the fabrication of spherical monosized Al particles. J Korean Powder Metall Inst. 2018;25(2):99-103. doi:10.4150/kpmi.2017.25.2.99.

[32] Yu Y, et al. The effect of the crucible on the temperature distribution for the growth of a large size AlN single crystal. Materials (Basel). 2022;15(1):54. doi:10.3390/ma15010054.

[33] Amrenova AZ, Dostiyarov AM, Yamanbekova AK, Umyshev DR, Ozhikenova ZF. Comparative study of NOx and CO formation during LPG combustion in a burner with different nozzles. Energies. 2025;18(18):4858. doi:10.3390/en18184858.

[34] Gupta AK. Flame characteristics with high temperature air combustion. American Institute of Aeronautics and Astronautics; 2000. Report No.: 0593.

[35] Zabihi A, Taghizadeh M. New energy-saving temperature controller for heater at natural gas gate station. J Nat Gas Sci Eng. 2015;27:1043-1049. doi:10.1016/j.jngse.2015.09.046.

[36] Ashouri E, Veysi F, Shojaeizadeh E, Asadi M. The minimum gas temperature at the inlet of regulators in natural gas pressure reduction stations (CGS) for energy saving in water bath heaters. J Nat Gas Sci Eng. 2014;21:230-240. doi:10.1016/j.jngse.2014.08.005.

[37] Pachpute SN. Combustion calculation for stoichiometry and flame properties [Internet]. CFD Flow Engineering; [cited 2026 Aug 14]. Available from: https://cfdflowengineering.com/combustion-calculation-for-stoichiometry-and-flame-properties/

[38] Al-Arkawazi SAF. Analyzing and predicting the relation between air-fuel ratio (AFR), lambda (λ) and the exhaust emissions percentages and values of gasoline-fueled vehicles using versatile and portable emissions measurement system tool. SN Appl Sci. 2019;1(11):1-12. doi:10.1007/s42452-019-1392-5.

[39] US Department of Energy. Check burner air to fuel ratios [Internet]. 2002. Available from: https://docs.nrel.gov/docs/fy02osti/31757.pdf

[40] Aliyu M, Nemitallah MA, Habib MA. Impact of excess air factor on performance and NOx emissions of an industrial water tube boiler with hydrogen enrichment. Eng Appl Comput Fluid Mech. 2024;2060:1-16. doi:10.1080/19942060.2024.2431102.

[41] US Department of Energy. Check burner air to fuel ratios [Internet]. 2007. Available from: https://energy.gov/sites/prod/files/2014/05/f16/check_burner_air2.pdf